

## LOW-MASS X-RAY BINARIES AND GLOBULAR CLUSTERS IN EARLY-TYPE GALAXIES. II. GLOBULAR CLUSTER CANDIDATES AND THEIR MASS-METALLICITY RELATION

PHILIP J. HUMPHREY<sup>1</sup>

*Accepted for publication in The Astrophysical Journal*

### ABSTRACT

We present an astrometry and photometry catalogue of globular cluster (GC) candidates detected with HST WFPC2 in a sample of 19 early-type galaxies, appropriate for comparison to the low-mass X-ray binary (LMXB) populations observed with *Chandra*. In a companion paper, we present the *Chandra* data and investigate the relation between these populations. We demonstrate that, although there is little evidence of a colour-magnitude correlation for the GCs, after estimating mass and metallicity from the photometry, under the assumption of a single age simple stellar population, there is a significant positive correlation between mass and metallicity. We constrained  $[Z/H] = (-2.1 \pm 0.2) + (0.25 \pm 0.04)\log_{10}M$ , with a  $1\text{-}\sigma$  intrinsic scatter of 0.62 dex in metallicity. If GCs are bimodal in metallicity this relation is consistent with recent suggestions of a mass-metallicity relation only for metal-poor clusters. Adopting a new technique to fit the GC luminosity function (GCLF) accounting for incompleteness and the Eddington bias, we compute the V-band local GC specific frequency ( $S_N$ ) and specific luminosity ( $S_L$ ) of each galaxy. We show that  $S_L$  is the more robust measure of the richness of a GC population where a significant fraction is undetected due to source detection incompleteness. We find that the absolute magnitude of the GCLF turnover exhibits intrinsic scatter from galaxy to galaxy of  $\sim 0.3$  mag ( $1\text{-}\sigma$ ), limiting its accuracy as a standard distance measure.

*Subject headings:* galaxies: elliptical and lenticular, cD— galaxies: star clusters— galaxies: general— galaxies: distances and redshifts

### 1. INTRODUCTION

Globular clusters (GCs) are found in galaxies of all morphological types and sizes. As primarily old stellar systems, their distribution and properties provide crucial insights into the way in which structure forms within the Universe. For a recent review we refer the reader to Brodie & Strader (2006). An intriguing characteristic of these objects, which provides valuable clues as to their structure and internal dynamics, is their association with low-mass X-ray binaries (LMXBs). Although it has long been recognized that LMXBs are overabundant per unit optical light by a factor  $\sim 100$  in Milky Way GCs as compared to the field (Fabian et al. 1975; Clark 1975), the small number of sources has limited what this phenomenon can tell us about LMXB formation. With the advent of *Chandra*, however, it has become feasible to resolve individual LMXBs in galaxies outside the Local Group, and thus to begin to assemble larger samples of LMXB-hosting GCs (e.g. Sarazin et al. 2003). Given their typically rich GC populations and their clean, old stellar populations which prevent contamination of the X-ray sources with high-mass X-ray binaries, massive early-type galaxies, in particular, provide an ideal environment in which to conduct such studies (e.g. Kundu et al. 2002; Sarazin et al. 2003; Humphrey & Buote 2004).

Even with the small samples of galaxies in which the GC-LMXB connection has been investigated to date, some intriguing trends have already been observed. By comparing the numbers of GCs and the total luminosity of LMXBs in early-type galaxies Irwin (2005) argued

that a significant fraction of the LMXBs observed in the field form in the field, despite the stellar population being old. Juett (2005) reported a similar result although, since they did not strictly compare the numbers of LMXBs and GCs within the same apertures, the strength of their correlation has been called into question (Kim et al. 2006). Typically  $\sim 4\%$  of GCs are observed to harbour LMXBs, with brighter and redder (more metal rich) GCs preferentially likely to contain them (Kundu et al. 2002; Sarazin et al. 2003; Kim et al. 2006). The GC luminosity dependence is broadly consistent with the probability of harbouring an LMXB being proportional to the mass or to the stellar capture cross-section in the GC (e.g. Jordán et al. 2004; Smits et al. 2006; Sivakoff et al. 2007). The origin of the colour dependence is unclear and several different possible explanations have been proposed (for a review of some of these, see Jordán et al. 2004). Maccarone et al. (2004) suggested it may relate to different patterns of mass-transfer in metal-rich and metal-poor LMXBs. Alternatively, it may arise due to variations in the IMF between metal-poor and metal-rich clusters (Grindlay 1987), or the efficiency of magnetic braking (Ivanova 2006). So far, however, most studies of the LMXB-GC connection have been relatively small and so strong general conclusions are difficult to draw.

The properties of the GC populations in early-type galaxies themselves are also of considerable interest since they provide a unique insight into how such galaxies form. Although the numbers of GCs do not simply scale with the total stellar mass of a galaxy, the GC luminosity function (GCLF) is observed to be remarkably uniform (e.g. Harris 1991). Typically it can be well-fitted by a log-normal distribution, the absolute shape of which varies

<sup>1</sup> Department of Physics and Astronomy, University of California, Irvine, 4129 Frederick Reines Hall, Irvine, CA 92697-4575

only weakly with the galaxy properties (e.g. Kundu & Whitmore 2001a; Jordán et al. 2006). The origin of this shape may be related to the dynamical destruction of low-mass GCs (e.g. Vesperini & Zepf 2003). The stability of the GCLF peak (“turnover”) has led to its adoption as a standard distance measure for nearby galaxies (Harris 1991; Jacoby et al. 1992), although there has been some debate as to its reliability (e.g. Ferrarese et al. 2000; Kundu & Whitmore 2001a). A recent study of early-type galaxies in Virgo (which span  $\sim 7$  magnitudes in B) by Jordán et al. (2007) found that the width and, possibly, the turnover magnitude vary with the galaxy absolute magnitude, in the sense that the least-massive galaxies have narrower, fainter GCLFs. The authors did, however, find significant scatter about these relations for galaxies at a given magnitude.

The GC colour distributions of early-type galaxies are observed to be almost universally bimodal, (e.g. Zepf & Ashman 1993; Gebhardt & Kissler-Patig 1999), probably indicating ubiquitous metal-rich and metal-poor sub-populations (although see Richtler 2006; Yoon et al. 2006). The GC distribution, in particular that of the metal-poor (i.e. blue) population, is observed to be substantially more extended than the optical light (Geisler et al. 1996). The average colour of the GCs in a galaxy strongly correlates with the total galaxy magnitude (Brodie & Huchra 1991), reflecting an increasing fraction of red GCs in more massive galaxies coupled with a correlation between mean GC metallicity and galaxy mass for both blue and red clusters (Peng et al. 2006). There is, however, no correspondingly strong correlation between the colour and luminosity of the GCs themselves (e.g. Larsen et al. 2001; Kundu & Whitmore 2001a). A weak colour-magnitude relation has been observed, but only in metal-poor GCs, in recent observations of nearby galaxies (Harris et al. 2006; Strader et al. 2006; Mieske et al. 2006). These clues point to different origins for the two sub-populations, with the metal-poor clusters possibly forming in low-mass halos in the very early Universe and being accreted during hierarchical structure formation. In contrast, metal rich clusters may form during the gas-rich mergers which assemble the massive galaxy (Brodie & Strader 2006, and references therein).

In this paper, we present a study of the GC populations in 19 early-type galaxies observed with *HST* WFPC2. In particular, we present a photometric catalogue of GC candidates which can be directly compared to the properties of observed LMXBs. In a companion paper, Humphrey & Buote (2008, hereafter Paper I), we present the *Chandra* data for these galaxies and investigate the relation between these populations, significantly expanding the sample of galaxies in which the LMXB-GC connection has been investigated. In the present work we compute self-consistently derived properties of the GC populations, such as the GC specific frequency,  $S_N$ , specific luminosity,  $S_L$ , and the GCLF turnover,  $m_V^T$ . The self-consistent computation of such parameters is essential for our analysis in Paper I. The galaxies used in this study were chosen from the *Chandra* and *HST* archives as having sufficiently deep ACIS and WFPC2 data to enable a significant fraction of the LMXBs and GCs to be individually resolved. To enable a consistent comparison between the galaxies and to mitigate against the rapidly-degrading *Chandra* PSF off-axis, we focus here

only on WFPC2 pointings of the centre of each galaxy. The galaxies, and the details of the archival observations used are shown in Table 1. All errors quoted are 90% confidence regions, unless otherwise stated in the text.

## 2. OBSERVATIONS AND DATA ANALYSIS

Data reduction and analysis were performed using the *Image Reduction and Analysis Facility*, IRAF (PC-IRAF vers. 2.12.2a), and the *Space Telescope Science Data Analysis System*, STSDAS (vers. 3.2) software suites. The individual pipelined images were first processed to correct for warm pixels with the *warmpix* STSDAS task. The corrected images were then aligned and, where the gain and filters were identical, combined with the STSDAS task *gcombine* to remove cosmic ray events. The alignment was achieved initially by examining the astrometry keywords in the data-file and shifting individual images an appropriate integer number of pixels. In a few cases the astrometry keywords were insufficiently accurate and so the offset between the images was determined by matching moderately bright point-sources between the exposures. In order to remove residual cosmic ray events and defective pixels which have not been removed in earlier processing (in particular since there are some pointings for which only a single exposure is available), the resulting images were processed with the LA-Cosmic<sup>2</sup> algorithm of van Dokkum (2001).

The detection of point sources against the bright, strongly-varying, “background” of galaxy emission is particularly challenging. To achieve this, we adopted a procedure similar to that outlined by Kundu et al. (1999, Kundu & Whitmore 2001a). First, to improve S/N, for each WFPC2 CCD we aligned and combined the images accumulated with different filters. An initial source list was created with the IRAF task *daofind*, having first estimated the statistical noise level from the region of the CCD with the least background galaxy emission and free from obvious point-sources. Due to the rapidly rising background across the WFPC2 field of view this procedure yields a very large number of detections, most of which are false on each CCD. To eliminate false detections, we recomputed the S/N for each source, based on local background estimates. To measure the source counts, we adopted a 3 pixel radius aperture and we estimated the background from an annulus with inner and outer radii of 3 and 5 pixels. We rejected any source with S/N lower than 4.8, implying only  $\sim 1$  false detection per CCD. In order to provide useful colour information, we required that any source was detected in all filters used. To eliminate spatially extended sources (most likely background galaxies), we excluded any source with a “concentration” (defined as the ratio of background-subtracted counts within a 3 pixel aperture to that within a 0.5 pixel aperture) outside the range 2–10. All detections were confirmed by visual inspection of the images.

To minimize confusion with small-scale but extended features (such as central dust-lanes) in the galaxies, which seriously complicate the computation of background-subtracted photometry, we eliminated detections within the central few arcseconds of each galaxy (shown in Table 1). In particular, data in the vicinity of a central nuclear disc in NGC 1387 and the bright

<sup>2</sup> Available at <http://www.astro.yale.edu/dokkum/lacosmic>

TABLE 1  
 TARGET LIST AND OBSERVATION LOG

Name	Type	Dist (Mpc)	$L_K$ ( $10^{11}L_\odot$ )	B			V			I			$R_{min}$ (")
				Filter	ObsID	Exp (s)	Filter	ObsID	Exp (s)	Filter	ObsID	Exp (s)	
NGC1332	S(s)0	21.3	1.4	...	...	...	F555W	u2tv03	160	F814W	u2tv03	320	2.9
NGC1387	SAB(s)0	18.9	0.78	...	...	...	F606W	u29r5h	160	...	...	...	8.7
NGC1399	cD	18.5	2.1	F450W	u34m02	2600	...	...	...	F814W	u34m02	1200	0.31
NGC1404	E1	19.5	1.5	F450W	u34m04	2400	...	...	...	F814W	u34m04	1260	1.7
NGC1553	SA(rl)0	17.2	1.9	...	...	...	F555W	u2tv28	160	F814W	u2tv28	320	2.0
NGC3115	S0	9.00	0.74	...	...	...	F555W	u2j20b	860	F814W	u2j20b	1236	2.7
NGC3585	E7/S0	18.6	1.5	...	...	...	F555W	u3m719	800	F814W	u3m719	1800	3.7
NGC3607	SA(s)0	21.2	1.5	...	...	...	F555W	u2tv12	160	F814W	u2tv12	320	8.4
NGC4125	E6pec	22.2	1.8	...	...	...	F555W	u3m723	1400	F814W	u3m723	2100	7.4
NGC4261	E2-3	29.3	2.2	...	...	...	F547M	u2i502	800	F791W	u2i502	800	1.6
NGC4365	E3	19.0	1.6	...	...	...	F555W	u2bm07	1000	F814W	u2bm07	460	3.5
NGC4472	E2/S0(2)	15.1	3.2	...	...	...	F555W	u66306	7200	F814W	u66315	5200	2.9
NGC4494	E1-2	15.8	0.81	...	...	...	F555W	u3vz05	1500	F814W	u3vz05	1800	2.3
NGC4552	E	14.3	0.85	...	...	...	F555W	u30708	1800	F814W	u30708	1500	0.85
NGC4621	E5	17.0	1.2	...	...	...	F555W	u2j20d	1380	F814W	u2j20d	830	6.4
NGC4649	E2	15.6	2.5	...	...	...	F555W	u2qo03	2100	F814W	u2qo03	2500	87.
NGC5018	E3	42.6	3.0	...	...	...	F555W	u3m725	800	F814W	u3m725	1800	4.3
NGC5845	E	24.0	0.27	...	...	...	F555W	u30709	2140	F814W	u30709	1120	3.8
NGC5846	E0-1	21.1	1.5	...	...	...	F555W	u36j04	1300	F814W	u36j04	1400	5.4

NOTE. — Summary of the sample galaxies and the observations used in the present analysis. The morphological type (Type) is taken from *NED*. All distances (Dist) are taken from Tonry et al. (2001), corrected by -0.16 mag to account for revisions to the Cepheid zero-point (e.g. Jensen et al. 2003), except that of NGC 5018, which was taken from Faber et al. (1989). Total, extrapolated  $K_s$ -band luminosities ( $L_K$ ) were taken from *2MASS* (Jarrett 2000), adopting  $M_{K_\odot} = 3.41$ . The zero-point was chosen for consistency with the stellar population models of Maraston (2005) (§ 3.2) and assuming the K-band and  $K_s$  band magnitudes do not differ significantly (e.g. Carpenter 2001). For each standard UBVR filter band, we list the observation ID (ObsID) of the WFPC2 datasets used, the actual filter used (Filter) and the total exposure in seconds (Exp). In addition, we show the approximate semi-major axis of the central, excluded region ( $R_{min}$ ).

knots of emission in the centre of NGC 4125 were excluded. The projection of the bright spiral NGC 4647 partly overlaps the image of NGC 4649, and so to minimize confusion we excluded any sources lying within the B-band twenty-fifth magnitude ellipse of NGC 4647, as listed in de Vaucouleurs et al. (1991).

Photometry was obtained with a 3 pixel radius aperture for the PC, and a 2 pixel aperture for the WF CCDs. The background was accumulated from an annulus between 3 and 5 pixels in radius. Since a GC may be slightly resolved in the case of the galaxies here, the proximity of the background annulus to the centre of the GC may lead to a slight over-subtraction and hence underestimate of the true brightness of a large GC. To estimate the likely magnitude of this effect, we simulated images of a GC at 15 Mpc, adopting a King (1962) model for its surface brightness profile. We adopted a ‘‘concentration’’ (the logarithm of the ratio between the truncation and core radii) of 1.25 and a half-light radius of 2.5 pc (e.g. Kundu et al. 1999). The images were convolved with images of the PSF for the wide field and planetary cameras, generated with the TinyTim<sup>3</sup> software package. For the planetary and wide field cameras, the magnitude of over-subtraction was  $\sim 0.1$  mag and  $\sim 0.02$  mag respectively. This magnitude is similar to the  $\lesssim 0.1$  mag error on the total magnitude of the GC estimated by Kundu et al. (1999) on account of typical GCs being slightly resolved at  $\sim 10$ – $20$  Mpc. These small effects will not significantly affect the interpretation of our results. Photometric zero-points were taken from Holtzman et al. (1995a), taking into account the appropriate gain correction. Aperture correction factors were estimated based on simulations using TinyTim for each CCD, assuming the spectrum

of a K4V star, and generally agreed with the calibration of Holtzman et al. (1995b). To estimate the extinction correction, we converted the line-of-sight estimates of Schlegel et al. (1998, listed in *NED*) to the wavelength of the mid-point of the appropriate filter, using the extinction law of Cardelli et al. (1989). This was typically very close to the Schlegel et al. value for the nearest standard photometric band. The photometry was converted to the standard UBVR system following the conversion formulae given in Holtzman et al. (1995a), assuming a standard V-I colour of 1.14 and a B-V colour of 0.97. For a consistent comparison between the galaxies, we converted the (B,I) band photometry of NGC 1399 and NGC 1404 into (V,I) band photometry by adopting the conversion formula given in Gebhardt & Kissler-Patig (1999).

### 3. GC COLOURS

#### 3.1. Colour Histograms

In order to investigate the colour distribution of GCs, we computed histograms of V-I colour for each galaxy. In Paper I we investigate the dependence of the probability that a GC hosts an LMXB as a function of metallicity, which we estimate by a simple transformation of the GC colour. Although, in general the colour distributions of GCs in early-type galaxies are bimodal, we do not expect whether a GC belongs to the red or blue subpopulation to affect its likelihood to host an LMXB, but rather this should depend on the metallicity. To obtain a global fit to this metallicity dependence in Paper I, we therefore need only to parameterize the composite colour distribution of all the GCs with a model which describes its *overall* shape reasonably well, and we do not need to capture the fine detail. As a simple approximation, we chose to adopt a single Gaussian model, which has previously

<sup>3</sup> Available at <http://www.stsci.edu/software/tinytim/>

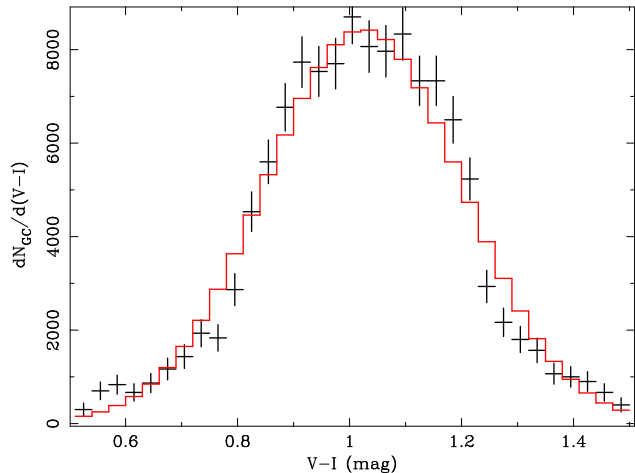


FIG. 1.— Composite GC colour distribution, fitted with a single Gaussian model. Although the model does not capture all of the fine detail of the distribution (which may be bimodal), it is a reasonable approximation of the overall shape.

been fitted to such data (e.g. Gebhardt & Kissler-Patig 1999). We show in Fig 1 the Gaussian fit to the composite GC colour histogram for all of the galaxies, with a mean  $V-I$  of  $1.033 \pm 0.005$  and  $\sigma$  of  $0.186 \pm 0.005$ . Although the fit is formally unacceptable ( $\chi^2/\text{dof}=57/27$ ), as is clear from Fig 1 the model does describe the global shape of the distribution reasonably well; in fact it is accurate to  $\sim 15\%$  for most of the interesting range of colours. This is adequate for our purposes in Paper I, as evinced by the excellent agreement we find in that paper between our measured metallicity dependence and that found by other authors with different techniques.

For comparison with other authors’ work, and to facilitate the comparison between galaxies in Paper I, we also fitted the single Gaussian model to the GC colour distributions of each galaxy. Given the fewer numbers of sources in each bin, we adopted a Cash-C minimization algorithm to fit the model to the data, and assessed the goodness-of-fit *via* 100 Monte-Carlo simulations. For each simulation, an artificial dataset was created given the best-fitting number of sources in each colour bin, which was then fitted with our preferred model. The fraction of simulations yielding a higher Cash-C statistic (i.e. worse fit) than the model fit to the real data can be used as an estimate of the goodness of fit. The fit was formally acceptable at a 5% significance level in most of the galaxies. Unacceptable fits were found for NGC 1399, NGC 3115, NGC 4494, NGC 4552, NGC 4621 and NGC 4649, which typically reflects evidence of bimodality or asymmetry in the GC colour distribution. Nonetheless, the fits of the single Gaussian model to the GC colour distributions of each galaxy (shown in Table 2) generally yield results consistent with those of Gebhardt & Kissler-Patig (1999), Kundu & Whitmore (2001a,b) or Larsen et al. (2001), where our sample overlapped with theirs.

### 3.2. Mass-metallicity relation

We show in Fig 2 (left panel) the composite colour-magnitude diagram for all of the GCs detected in more than one filter. We also show representative error-bars and the data rebinned into a series of narrow magnitude bins. The data do not show convincing evidence of a sig-

nificant colour-magnitude correlation. For example, the binned-up data are consistent ( $\chi^2/\text{dof}=13.6/8$ ) with no variation in colour with magnitude. The fit does not improve significantly ( $\chi^2=12.2/7$ ) when fitted with a linear model of the form  $(V - I) = (1.043^{+0.014}_{-0.005}) + (0.003 \pm 0.005)V$ ; this is consistent with no variation within errors and indicates that, if any correlation is present, it is extremely weak. The  $V-I$  colour used in the present work does not cleanly separate the metal-poor and metal-rich sub-populations of GCs; coupled with the small field of view of the WFPC2, which limits the numbers of blue GCs detected, we do not see the so-called “blue tilt” (i.e. colour-magnitude correlation) recently observed in the metal-poor GC populations of several galaxies (Harris et al. 2006; Strader et al. 2006).

In the right panel of Fig 2, we show the same data converted into mass and metallicity. To achieve this, we linearly interpolated the  $V$  and  $I$ -band photometry onto the updated simple stellar population (SSP) model grids of Maraston (2005, see also Maraston 1998)<sup>4</sup>. We adopted these models for consistency with our previous study of the mass and metallicity of early-type galaxies, in which we adopted the alpha-enhanced Lick index models of Thomas et al. (2003), built upon these SSP models (Humphrey & Buote 2006). In our study of the mass profiles of early-type galaxies, Humphrey et al. (2006), we found that our measured  $K$ -band mass-to-light ratios in the (baryon-dominated) centres of the galaxies were consistent with the predictions of the Maraston models, provided one adopted a Kroupa (2001) initial mass function, which we therefore adopted in the present work. Maraston provides the mass-to-light ratio as a function of metallicity and age. We assumed an age of 13 Gyr, and adopted the SSP models computed for a Kroupa initial mass function and a blue horizontal branch (HB) for the GC stars. A small fraction of the GCs with best-fitting abundances pegged at the high or low boundaries ( $[Z/H]=-2.25$  and  $0.67$ , respectively) were discounted. Since the  $V$  and  $I$ -band mass-to-light ratios show a dependence upon the metallicity, the *lack* of a correlation between  $V-I$  and  $V$  actually translates into a slight mass-metallicity correlation. Formal correlation testing was carried out using three different methods, Pearson’s linear correlation test, Spearman’s rank-order test and Kendal’s  $\tau$  test. All three tests indicated that the probability of no correlation is less than  $10^{-29}$ .

We also show in Fig 2 the data binned into a series of narrow mass bands. The error-bars on the mean GC metallicity in each bin were estimated from the  $1-\sigma$  scatter of the data-points, using the central limit theorem. These data are well-fitted ( $\chi^2/\text{dof}=4.3/5$ ) by a simple linear model of the form  $[Z/H] = (-2.1 \pm 0.2) + (0.25 \pm 0.04)\log_{10}M$ , where  $M$  is the mean GC mass. To estimate the intrinsic scatter about this best-fitting relation, we additionally fitted this model to the  $y$ -on- $x$  data-points for each GC, taking into account the errors on both axes with an algorithm similar to that outlined in Press et al. (1992, see also Tremaine et al. 2002). We added in quadrature with the metallicity error an additional, constant, systematic error-term,

<sup>4</sup> [http://www-astro.physics.ox.ac.uk/~maraston/Claudia's\\_Stellar\\_Population\\_Models.html](http://www-astro.physics.ox.ac.uk/~maraston/Claudia's_Stellar_Population_Models.html)

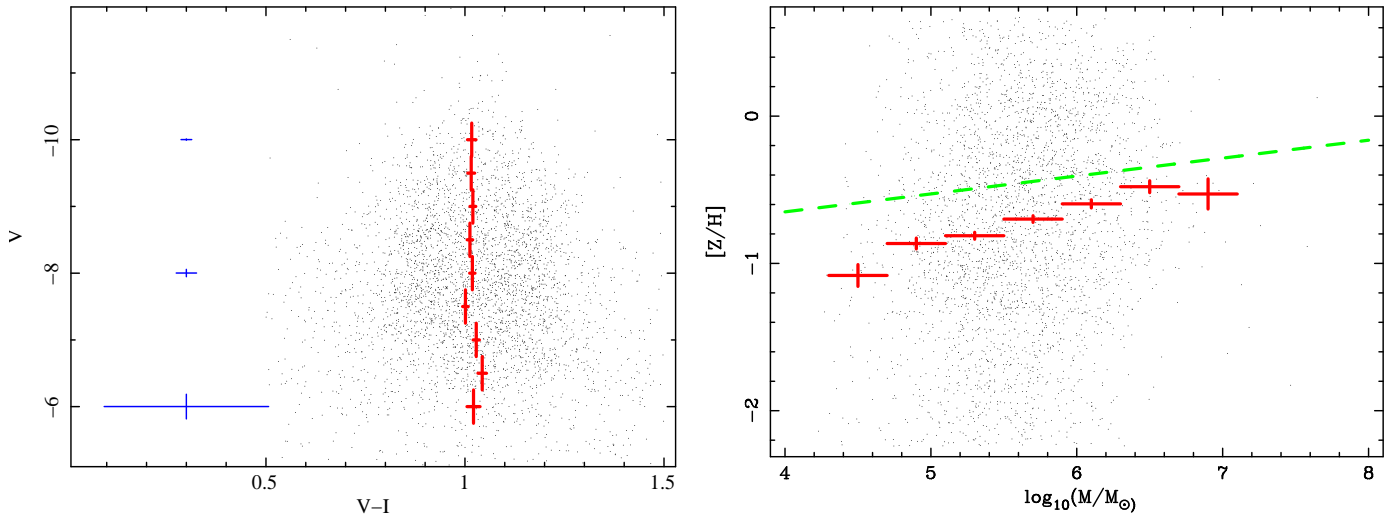


FIG. 2.— Left: Composite colour-magnitude diagram for all of the GC candidates. We show (blue) representative error-bars for a range of V magnitudes. Overlaid we show the data-points binned into a series of magnitude bins, clearly indicating little or no colour-magnitude relation. Right: the same data, transformed into mass and metallicity space (see text). Overlaid we show the same data binned into a series of metallicity bins, clearly indicating a slight mass-metallicity correlation. We also show (dotted line) an extrapolation of the best-fitting mass-metallicity relation for early-type galaxies found by Thomas et al. (2005)

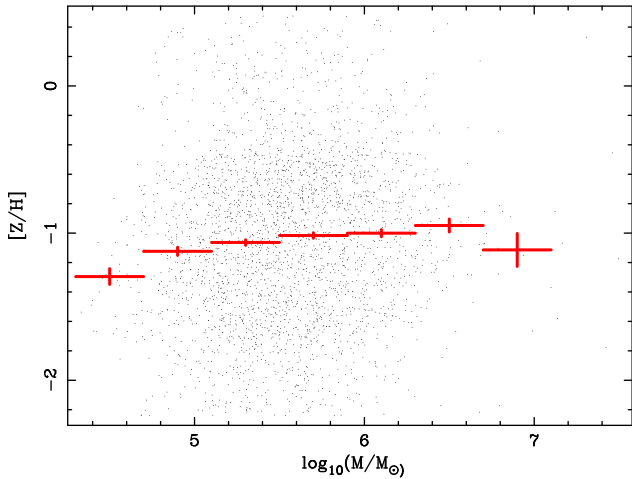


FIG. 3.— Same as Fig 2, right panel, but using the PEGASE SSP models to convert colour and magnitude to mass and metallicity.

which was adjusted until the  $\chi^2/\text{dof}$  value was 1, at which point its value is approximately equal to the  $1\text{-}\sigma$  intrinsic scatter about the best-fitting linear relation. In this way, we estimated this scatter to be 0.62 dex in metallicity.

Since the assumption of a blue HB is most appropriate for metal-poor GCs, we have investigated the impact of using the red HB models instead of the blue models. We found that this produces a small shift in [Z/H], at maximum  $\sim 0.2$  dex, which does not appear to correlate with mass. We found similar shifts (albeit typically of a different sign) if we adopted a GC age of 10 Gyr. We therefore conclude that relaxing our assumptions of a fixed GC age or a blue HB for all GCs is unlikely to make the observed trend disappear. In order to verify that our results do not sensitivity depend upon the choice of SSP models, we also experimented with adopting models based on the **PEGASE.2** code of Fioc & Rocca-Volmerange (1997, 1999) to perform the transformation from colour to mass and metallicity space. We took most of the default parameters of the code, adopted a Kroupa IMF, assumed a single burst of star-formation

and we included the mass of neutron-stars and white dwarfs in the calculation of the mass-to-light ratio. For consistency with the Maraston models, we adopted approximately the same transformation between the heavy element mass fraction (“Z”) and [Z/H] as those authors. The resulting mass-metallicity plot is shown in Fig 3. We also show the data binned into a series of narrow mass bands, which clearly indicates a mass-metallicity correlation similar to that found above. Fitting the binned data with a simple linear model, we found that the data are inconsistent with a constant [Z/H] model ( $\chi^2/\text{dof}=42/6$ ), but are in agreement ( $\chi^2/\text{dof}=11/5$ ) with a model of the form  $[Z/H] = (-1.8 \pm 0.2) + (0.12 \pm 0.03)\log_{10}M$ . Both the slope and normalization of the best-fitting model differ from the relation obtained with the Maraston models, which reflects quantitative differences in the relation between the mass-to-light ratios and the metallicity for the two sets of models.

#### 4. LUMINOSITY FUNCTIONS

##### 4.1. Source Detection Incompleteness

In order to measure accurately the GCLF in each galaxy it is essential to take into account the source detection incompleteness. The ability of the algorithm outlined in § 2 to detect point-sources is a strong function both of the source flux and the “background” level, which varies dramatically over the WFPC2 field of view. It is therefore certain that some fraction of the GCs in any given galaxy will not be detected. To estimate the completeness of our source lists, we therefore carried out extensive Monte-Carlo simulations. Starting with the V-magnitude (B-band for NGC 1404 and NGC 1399) of the faintest sources detected in each galaxy, we stepped through a series of magnitude bins, each separated by 0.2 mag, in each of which we performed 10 Monte-Carlo simulations to estimate the completeness level. We have explicitly confirmed that starting from one magnitude fainter than this limit makes no measurable difference to our key results for one galaxy, NGC 4649. Each simulation entailed the addition of ten simulated point sources

TABLE 2  
DERIVED PROPERTIES OF THE GC POPULATIONS

Name	$N_{GC}^{det}$	$V - I_0$	$\sigma_{V-I}$	$f_i^{GC}$	$L_{GC}$ ( $10^7 L_\odot$ )	$L_V^{FOV}$ ( $10^{10} L_\odot$ )	$m_V^T$	$S_N$	$S_L$
NGC1332	198	$0.998 \pm 0.03$	$0.22^{+0.03}_{-0.02}$	0.60	$8.3 \pm 1.2$	$2.0 \pm 0.9$	$24.4 \pm 0.4$	$2.5 \pm 1.1$	$0.42 \pm 0.19$
NGC1387	28	...	...	0.22	$0.79 \pm 0.51$	$1.2 \pm 0.3$	...	$0.38 \pm 0.26$	$0.065 \pm 0.045$
NGC1399	467	$1.034 \pm 0.009$	$0.123^{+0.007}_{-0.006}$	0.81	$12. \pm 1.$	$2.0 \pm 1.8$	$24.0 \pm 0.2$	$3.5 \pm 3.1$	$0.59 \pm 0.53$
NGC1404	109	$1.01 \pm 0.02$	$0.14 \pm 0.01$	0.74	$5.3 \pm 0.9$	$1.7 \pm 1.8$	$24.3 \pm 0.4$	$1.8 \pm 2.0$	$0.32 \pm 0.35$
NGC1553	71	$0.996 \pm 0.04$	$0.19^{+0.04}_{-0.03}$	0.76	$2.1 \pm 0.5$	$2.7 \pm 0.6$	$24.5 \pm 0.6$	$0.45 \pm 0.14$	$0.077 \pm 0.024$
NGC3115	136	$1.01 \pm 0.02$	$0.15^{+0.02}_{-0.01}$	0.92	$2.3 \pm 0.4$	$1.1 \pm 0.1$	$22.7 \pm 0.3$	$1.2 \pm 0.3$	$0.21 \pm 0.04$
NGC3585	90	$0.99 \pm 0.04$	$0.23^{+0.05}_{-0.03}$	0.83	$2.4 \pm 0.4$	$3.0 \pm 0.8$	$24.6 \pm 0.4$	$0.47 \pm 0.15$	$0.081 \pm 0.026$
NGC3607	106	$0.95 \pm 0.03$	$0.19^{+0.03}_{-0.02}$	0.62	$4.9 \pm 0.9$	$2.4 \pm 0.8$	$24.0 \pm 0.4$	$1.2 \pm 0.4$	$0.20 \pm 0.07$
NGC4125	196	$1.05 \pm 0.03$	$0.24^{+0.04}_{-0.03}$	0.74	$2.6 \pm 0.4$	$3.2 \pm 0.8$	$25.5 \pm 0.3$	$1.3 \pm 0.5$	$0.082 \pm 0.023$
NGC4261	241	$1.00 \pm 0.02$	$0.20 \pm 0.02$	0.56	$11. \pm 1.$	$3.4 \pm 3.4$	$24.6 \pm 0.3$	$2.0 \pm 2.0$	$0.34 \pm 0.34$
NGC4365	291	$1.01 \pm 0.02$	$0.18 \pm 0.01$	0.81	$8.2 \pm 0.9$	$2.3 \pm 0.6$	$24.0 \pm 0.2$	$2.1 \pm 0.6$	$0.36 \pm 0.11$
NGC4472	397	$1.08 \pm 0.02$	$0.18 \pm 0.01$	0.83	$7.1 \pm 0.7$	$3.9 \pm 0.5$	$23.8 \pm 0.2$	$1.1 \pm 0.2$	$0.18 \pm 0.03$
NGC4494	155	$0.98 \pm 0.02$	$0.18 \pm 0.02$	0.86	$3.0 \pm 0.4$	$1.5 \pm 0.5$	$23.5 \pm 0.2$	$1.2 \pm 0.4$	$0.20 \pm 0.07$
NGC4552	240	$1.02 \pm 0.02$	$0.18^{+0.02}_{-0.01}$	0.85	$4.2 \pm 0.5$	$1.3 \pm 0.4$	$23.4 \pm 0.2$	$1.9 \pm 0.6$	$0.32 \pm 0.10$
NGC4621	173	$1.04 \pm 0.02$	$0.15^{+0.02}_{-0.01}$	0.86	$3.9 \pm 0.5$	$1.7 \pm 0.5$	$23.4 \pm 0.2$	$1.3 \pm 0.4$	$0.23 \pm 0.07$
NGC4649	323	$1.05 \pm 0.02$	$0.17 \pm 0.01$	0.87	$6.8 \pm 0.7$	$2.9 \pm 0.4$	$23.6 \pm 0.2$	$1.4 \pm 0.3$	$0.23 \pm 0.04$
NGC5018	90	$0.87^{+0.04}_{-0.05}$	$0.21^{+0.05}_{-0.03}$	0.47	$7.8 \pm 1.8$	$9.7 \pm 4.1$	$25.1^{+0.6}_{-0.5}$	$0.46 \pm 0.22$	$0.080 \pm 0.038$
NGC5845	45	$0.96^{+0.08}_{-0.15}$	$0.29^{+0.19}_{-0.07}$	0.47	$1.4 \pm 0.8$	$1.9 \pm 1.1$	...	$0.45 \pm 0.36$	$0.077 \pm 0.062$
NGC5846	288	$1.04 \pm 0.02$	$0.18^{+0.02}_{-0.01}$	0.76	$5.3 \pm 0.6$	$2.6 \pm 1.1$	$24.8 \pm 0.2$	$1.4 \pm 0.6$	$0.21 \pm 0.09$

NOTE. — Derived properties of each of the galaxies' GC distributions. We list the number of GCs detected ( $N_{GC}^{det}$ ), the mean colour of the GCs ( $V-I_0$ ), the half-width of the V-I distribution ( $\sigma_{V-I}$ ), the total fraction of the GC luminosity which has been detected ( $f_i^{GC}$ ), the total V-band luminosity of the GCs, correcting for incompleteness ( $L_{GC}$ ), the V-band magnitude of the galaxy in the field of view ( $L_V^{FOV}$ ), the V-band GCLF turnover ( $m_V^T$ ), the specific frequency of GCs ( $S_N$ ) and the specific luminosity ( $S_L$ ). The correlations between these properties and the LMXB distribution are discussed in detail in Paper I. All quoted errors are 90% confidence limits, incorporating only statistical uncertainties. An assessment of statistical errors is given in Table 3.

TABLE 3  
SYSTEMATIC ERROR-BUDGET FOR DERIVED PARAMETERS

Name	$f_i^{GC}$ $\Delta_{free}$	$\Delta_{wid}$	$L_{GC}$ $\Delta_{stat}$	$\Delta_{free}$	$\Delta_{wid}$	$S_N$ $\Delta_{stat}$	$\Delta_{free}$	$\Delta_{wid}$	$S_L$ $\Delta_{stat}$	$\Delta_{free}$	$\Delta_{wid}$
NGC1332	-0.052	-0.063	1.2	0.83	0.98	1.1	1.5	1.4	0.19	0.042	0.050
NGC1387	...	$-4.8 \times 10^{-4}$	0.51	...	$3.9 \times 10^{-3}$	0.26	...	0.71	0.045	...	$3.2 \times 10^{-4}$
NGC1399	-0.021	-0.049	1.0	-0.50	0.88	3.1	0.97	1.0	0.53	-0.025	0.043
NGC1404	-0.068	-0.055	0.86	-0.18	0.36	2.0	0.77	1.3	0.35	-0.011	0.021
NGC1553	-0.18	-0.18	0.48	0.14	0.20	0.14	0.74	0.91	0.024	$5.0 \times 10^{-3}$	$7.4 \times 10^{-3}$
NGC3115	-0.022	-0.039	0.36	-0.46	-0.14	0.23	0.29	0.32	0.040	-0.040	-0.012
NGC3585	-0.095	-0.11	0.44	-0.42	-0.23	0.15	0.31	0.47	0.026	-0.014	$-7.7 \times 10^{-3}$
NGC3607	-0.016	$-7.6 \times 10^{-4}$	0.93	0.29	0.61	0.43	0.21	0.18	0.074	0.012	0.025
NGC4125	...	-0.089	0.37	...	0.27	0.53	...	0.61	0.023	...	$8.5 \times 10^{-3}$
NGC4261	-0.11	-0.032	1.5	3.7	1.7	2.0	2.6	-0.023	0.34	0.11	0.050
NGC4365	-0.043	-0.016	0.86	0.044	0.80	0.61	0.59	0.59	0.11	$1.9 \times 10^{-3}$	0.035
NGC4472	-0.035	-0.042	0.69	-1.3	0.051	0.16	0.55	0.30	0.028	-0.034	$1.3 \times 10^{-3}$
NGC4494	$-3.5 \times 10^{-3}$	-0.085	0.42	-0.32	0.95	0.42	0.41	0.053	0.071	-0.022	0.065
NGC4552	-0.032	-0.060	0.51	-0.61	0.66	0.57	0.95	0.20	0.098	-0.046	0.051
NGC4621	0.011	-0.014	0.51	0.87	1.8	0.40	-0.039	-0.066	0.069	0.051	0.11
NGC4649	-0.017	-0.014	0.68	0.22	1.5	0.25	0.19	0.23	0.041	$7.6 \times 10^{-3}$	0.050
NGC5018	-0.011	0.097	1.8	1.2	0.043	0.22	0.10	-0.13	0.038	0.013	$4.4 \times 10^{-4}$
NGC5845	...	-0.019	0.59	...	0.59	0.43	...	$7.4 \times 10^{-3}$	0.073	...	0.045
NGC5846	-0.014	-0.048	0.57	-0.74	-0.090	0.62	0.64	0.61	0.088	-0.029	$-3.5 \times 10^{-3}$

NOTE. — Error-budget for  $f_i^{GC}$ ,  $L_{GC}$ ,  $S_N$  and  $S_L$ , showing the statistical errors ( $\Delta_{stat}$ ) and an estimate of the impact on the parameters from allowing the GCLF turnover to fit freely while fitting all of the available data ( $\Delta_{free}$ ) or from adopting a GCLF width of 1.5 mag ( $\Delta_{wid}$ ); see text. We indicate by ellipses cases where the data could not be constrained (NGC 1387 and NGC 5845) or where the parameters were already derived allowing the GCLF turnover to be free (NGC 4125).

to the actual WFPC2 images of the galaxy in each filter. The V-I colours of the sources were chosen randomly by drawing, with replacement, from the V-I distribution of the detected sources. The source detection algorithm was run on each image and the number of simulated sources which were detected, as well as their measured magnitudes, was determined. Once 98 percent of the simulated sources were detected in any bin, the simulations were stopped and all sources brighter than the corresponding magnitude were assumed detected at their true magnitude (this is, in general, a very good approximation since the measurement errors on the brightest GCs are typically much less than the 0.2 mag binsize we adopt). The sources were assumed to be distributed as the optical light, which, for these purposes was modelled as an elliptical de Vaucouleurs profile centred at the peak of the galaxy emission, with the size and orientation given in de Vaucouleurs et al. (1991, except for NGC 1332, for which the position angle was modified to match better the observed image of the galaxy). Point-source images were generated with the TinyTim tool for the appropriate filter and focal plane position of the source, assuming the spectrum of a K4V star.

Any given parameterization of the GCLF which we fit predicts the number of sources which should, in the idealized case, be observed in any given magnitude bin. To account for incompleteness and statistical errors, this model was convolved, in each bin, with a function, determined from our simulations, which redistributes the sources into adjacent bins, based on the likelihood it is detected in each magnitude bin. The corrected model can then be fitted directly to the data. This method is exactly analogous to computing a “response matrix”, through which any parameterized model can be folded in X-ray spectral-fitting (e.g. Davis 2001). We discuss this method, and the intrinsic uncertainty associated with our method of computing the matrix in Appendix A. This procedure not only accounts for source detection incompleteness, but also the Eddington bias, while preserving the statistical integrity of the data.

#### 4.2. Fitting the GCLFs

For each galaxy, we accumulated a V-band (B-band for NGC 1399 and NGC 1404) GCLF by constructing a histogram of the numbers of sources observed in a series of magnitude bins of width 0.2 mag. We created an associated response matrix, as described in Appendix A and fitted the data with dedicated software through a Cash-C statistic function minimization procedure. We modelled the GC magnitude distribution as a simple Gaussian, i.e.

$$\frac{dn_{GC}}{dV} = \frac{N_{TOT}}{\sqrt{2\pi}\sigma_V} \exp\left(-\frac{(V - V_T)^2}{2\sigma_V^2}\right) \quad (1)$$

where  $n_{GC}$  is the number density of GCs, as a function of V-band luminosity ( $V$ ),  $N_{TOT}$  is the total number of GCs and  $V_T$  is the apparent V-band peak luminosity (“GCLF turnover”). This has been previously shown to be a reasonable description of the GCLF shape (e.g. Harris 1991; Kundu & Whitmore 2001a). For consistency with past analysis, and to minimize the sensitivity of our results to the our source detection incompleteness algorithm, we initially fitted only those data-bins for which the source detection completeness was estimated to be 50%

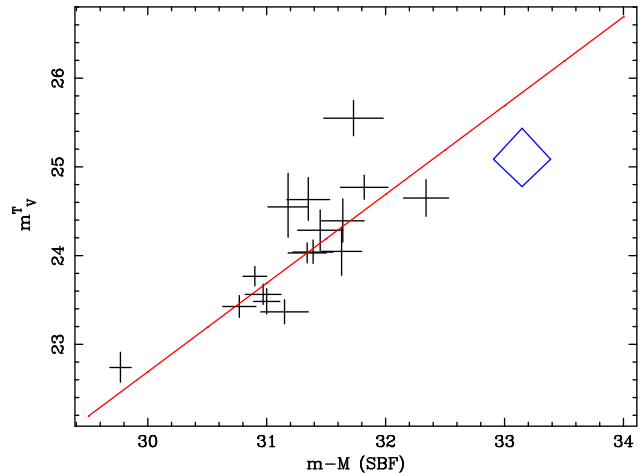


FIG. 4.— Comparison of the measured GCLF turnover and the corrected I-band SBF distance moduli (Table 1). NGC 5018, for which the distance was derived from the  $D_n$ - $\sigma$  relation (Faber et al. 1989), is shown as a diamond. The straight line denotes the best-fitting straight line relation (see text), which is consistent with previously-reported correlations. This demonstrates the utility of the GCLF turnover magnitude as an approximate “standard candle”.

or greater. In general, our incompleteness cut allowed insufficient data below the GCLF turnover to constrain all three parameters of the Gaussian fit and so, based on past work (Kundu & Whitmore 2001a; Jordán et al. 2006), we fixed the GCLF half-width ( $\sigma_V$ ) to 1.3 mag. This should be a reasonable average value for giant elliptical galaxies, although in individual objects significantly broader or narrower GCLFs may exist.

In Table 2 we list the V-band turnover magnitude,  $m_V^T$  for each galaxy. To enable a consistent comparison, we convert B-band turnover magnitudes for NGC 1399 and NGC 1404 to the V-band by assuming a constant B-V of 0.97, consistent with the colours of these galaxies, and also consistent with a  $\sim$ solar metallicity 10 Gyr stellar population (Maraston 2005). We ignored NGC 1387 and NGC 5845, for which there were too few measured GCs to make the GCLF turnover measured in this way reliable. Where our samples overlap, our measured  $m_V^T$  were in good agreement with those found by Kundu & Whitmore (2001a,b) and Larsen et al. (2001, who fitted a slightly different functional form to the GCLF), giving us confidence in our fitting procedure.

In Fig 4 we show  $m_V^T$  as a function of the distance modulus. Taking into account errors on both the x and y data values we fitted the data with a function of the form  $m_V^T = (m - M)_{SBF} + M_V^T$ , where  $M_V^T$ , the absolute turnover magnitude, was fitted freely. The fit was formally unacceptable ( $\chi^2/\text{dof}=35/16$ ), indicating significantly more scatter about this relation than the statistical errors. Omitting the most discrepant data-point, that of NGC 4125, significantly improved the fit ( $\chi^2/\text{dof}=23/15$ ), although it remained only marginally acceptable. For this fit we constrained  $M_V^T = -7.30 \pm 0.05$ , in good agreement with previous estimates (e.g. Kundu & Whitmore 2001a), especially when we account for recent revisions to the Cepheid zero-point (e.g. Jensen et al. 2003). In general, however, the *ad hoc* removal of data-points should be avoided. Taking our fit to NGC 4125 at face value implies intrinsic scatter (estimated as described in § 3.2) of 0.4 mag, with a 90% lower limit of

0.26 mag, and a best-fitting  $M_V^T$  of  $-7.26 \pm 0.15$ .

In order to compare the LMXB and GC populations in Paper I, we require an estimate of the fraction of the GC luminosity which is detected in the WFPC2 field of view,  $f_i^{GC}$ . To estimate this for each galaxy, we adopted the canonical GCLF ( $M_V^T = -7.3$ ,  $\sigma_V = 1.3$ ) to each dataset (except for NGC 4125, for which we adopted  $M_V^T$  derived from fitting) and computed the observed and total luminosity of GCs by appropriately integrating the incompleteness-corrected and the uncorrected models. We tabulate  $f_i^{GC}$  in Table 2.

#### 4.3. Specific frequency and luminosity

To quantify the richness of the GC populations of each galaxy within the WFPC2 aperture, we computed two quantities, the GC specific frequency,  $S_N$ , and the GC specific luminosity,  $S_L$  (e.g. Harris 1991), defined by the relations:

$$S_N = N_{GC} 10^{0.4(M_V^{FOV} + 15)} \quad (2)$$

$$S_L = 100 L_{GC} / L_V^{FOV} \quad (3)$$

where  $N_{GC}$  is the total number of GCs inferred from fitting the GCLF,  $L_{GC}$  is the total luminosity of the GCs inferred from the fit,  $M_V^{FOV}$  is the V-band absolute magnitude of the galaxy in the field of view and  $L_V^{FOV}$  is the corresponding luminosity. Although we find significant intrinsic scatter in  $M_V^T$ , in order to produce interesting constraints, we computed  $N_{GC}$  and  $L_{GC}$  having fixed  $M_V^T$  to  $-7.3$  for each galaxy, except for NGC 4125, for which we allowed the turnover to fit freely since it is substantially fainter than  $M_V^T$  (Fig 4). We estimated  $M_V^{FOV}$ , following Kundu & Whitmore (2001a), by integrating the total counts in the field of view (having excluded obvious bright interloper sources) and adopting a background level of 0.01 and  $0.052 e^- s^{-1} pixel^{-1}$  for the PC and WF CCDs. We computed these quantities in the V-band for all galaxies, excepting NGC 1399 and NGC 1404, for which they were computed in the B-band. For these two systems, we subsequently corrected  $S_N$  to the V-band, assuming a galaxy B-V colour of 0.97. The best-fitting results are shown in Table 2. Where our data overlap, our computed  $S_N$  (shown in Table 2) generally agree very well with those reported by Kundu & Whitmore (2001a,b). The GCLF data and the best-fitting models are shown in Fig 5.

This model fits the data brighter than the cut-off well. However, extrapolation to fainter magnitudes generally reveals some discrepancies (Fig 5). This may reflect actual differences between the GCLF width and our canonical  $\sigma_V = 1.3$  mag, the increasing importance of (and difficulty in eliminating) interlopers at faint magnitudes, and possible deficiencies in our incompleteness-estimation algorithm. To investigate how important these effects may be, we experimented with fitting all of the data-points and freeing  $M_V^T$ . The best-fitting models for such fits are shown (dashed lines) in Fig 5. In Table 3, we tabulate the systematic uncertainties on  $S_N$  and  $S_L$  arising from this choice or, similarly, fixing the GCLF width to  $\sigma_V = 1.5$  (see § 4.4). Another potential source of systematic uncertainty is the assumed spatial distribution of the point sources in our simulations. In order to assess how significantly this may affect our results, we recomputed

the incompleteness correction for one system, NGC 4649, but distributing the simulated sources as a  $\beta$  model, with  $\beta = 0.46$  and core radius  $0.81'$ . Such a model approximately fits the distribution of the LMXBs in this system. We found  $S_N$  changed by 0.20 and  $S_L$  by 0.026, which are consistent with the statistical errors, and other sources of systematic uncertainty for this object. In general, since  $S_L$  is more sensitive to the bright end of the GCLF distribution, we found it was more robust than  $S_N$  to these choices; the systematic effect on  $S_N$  of freeing  $M_V^T$  was generally larger than the statistical errors, whereas the impact on  $S_L$ , while not negligible, was typically smaller than, or comparable to, the statistical errors.  $S_L$  also has the advantage that it is independent of the any error in the assumed distance to the galaxy.

#### 4.4. Composite GCLF

In Paper I we investigate the dependence of LMXBs in GCs by comparing the composite luminosity function of the GCs in all galaxies with that of the GCs containing LMXBs. In order to investigate the composite GCLF, we first computed V-band GCLFs for each galaxy in a set of standard absolute magnitude bins, and appropriate response files, as described in § 4.1. To mitigate against the intrinsic scatter in  $M_V^T$ , for each galaxy we adopted a distance modulus given by the measured  $m_V^T + 7.3$  to convert from apparent to absolute magnitude. To take account of incompleteness effects the response matrices were averaged using the *Heasoft* tool *addrmf*, weighting each matrix by the number of detected sources. To enable us to combine the GCLFs for NGC 1399 and NGC 1404 with the other data, we converted from the B to V band by assuming a constant B-V=0.97.

The combined GCLF was well-fitted by a single Gaussian model, with  $\sigma_V = 1.51 \pm 0.04$ . The data and best-fitting model are shown in Fig 6. We note that the best-fitting  $\sigma_V$  is slightly larger than our adopted 1.3 mag used in computing  $S_N$  and  $S_L$ . This most likely arises due to the GCLFs of some, although not necessarily all, of the objects being slightly broader than we have assumed. The nature of a composite GCLF is that its shape is heavily biased towards the most GC-rich galaxies, and so  $\sigma_V = 1.5$  need not be representative of the majority of the galaxies in our sample. Kundu & Whitmore (2001a) found that NGC 4472 and NGC 4649, which account for  $\sim 20\%$  of the detected GCs, may have  $\sigma_V \gtrsim 1.5$ . The GCLF-determined distance moduli have statistical uncertainties typically of the order  $\sim 0.1-0.2$  ( $1-\sigma$ ), which should also cause the measured composite GCLF to be slightly broadened. Nonetheless, we estimate in Table 3 the systematic effect on the best-fitting  $S_N$  and  $S_L$  of fixing  $\sigma_V = 1.5$ .

### 5. SPATIAL DISTRIBUTION OF GLOBULAR CLUSTERS

In order to investigate the spatial distribution of the GCs, we separately binned radial distributions for the red and blue GCs, defining any cluster with  $V-I > 1.1$  as red, and the remaining clusters as blue. We note that this does not cleanly separate the blue and red sub-populations of clusters and so measured differences in the spatial distributions probably underestimate intrinsic differences between the red and blue sub-populations. However, it does divide clusters on the basis of their *actual* metallicity (rather than asking to which subpopula-



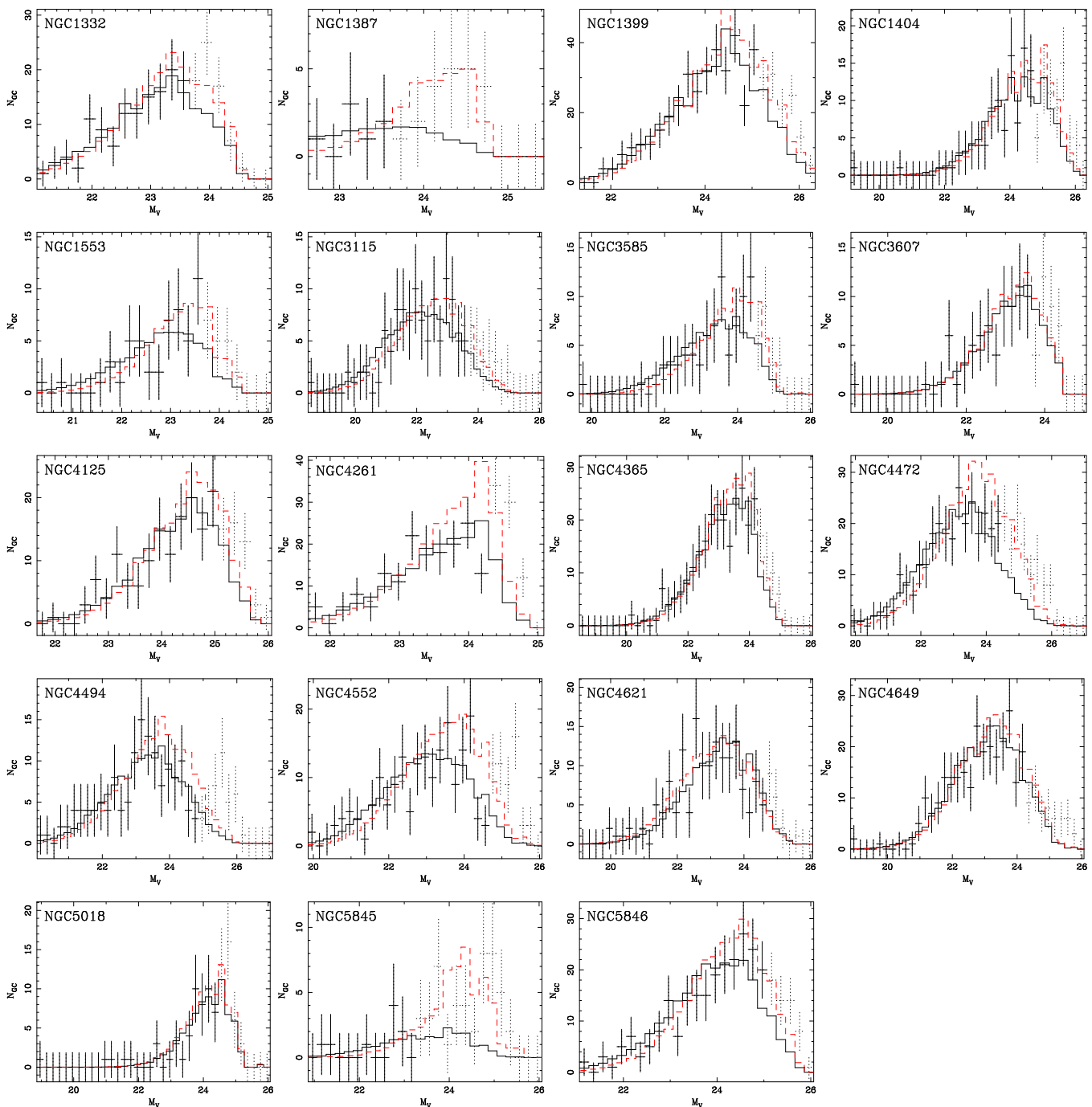


FIG. 5.— GCLFs of each of the galaxies in the sample, shown with the best-fit Gaussian model (solid line), corrected for source detection incompleteness. Data-bins for which source detection completeness was below 50% (not included in the fit) are drawn with dotted lines. The dashed line shows the best-fitting model if all of the data are fitted and the turnover magnitude is allowed to fit freely. Although the data were fitted by minimizing the Cash-C statistic, we show error-bars estimated from Gehrels’ approximation (for the upper limit) to guide the eye. In most cases the data are well-represented by the simple Gaussian model, and the results are not highly sensitive to the inclusion or exclusion of the more sources at the uncertain faint end of the GCLF.

tion they belong), thereby allowing us to assess whether, for our galaxies, more metal-rich clusters are, on average, distributed differently to more metal-poor ones. This distinction is extremely important when comparing to the spatial distribution of LMXBs (Paper I).

To compute the radial profile, the radial distances of each source from the optical centre of the galaxy, identified by eye, were binned into a set of 7 radial bins, with outer annuli 0.33, 0.66, 0.82, 1.0, 1.2, 1.3 and 1.5’, re-

spectively. The data were rebinned to ensure at least 3 sources per bin and the radial distribution was fitted with a variety of models by a Cash-C statistic minimization algorithm. To correct the spatial distributions of sources for detection incompleteness, we computed a GCLF correction function, similar to that described in § 4.1 for each bin. Assuming the GCLF does not vary spatially, this correction was combined with the measured GCLF for that galaxy to estimate the fraction of sources which

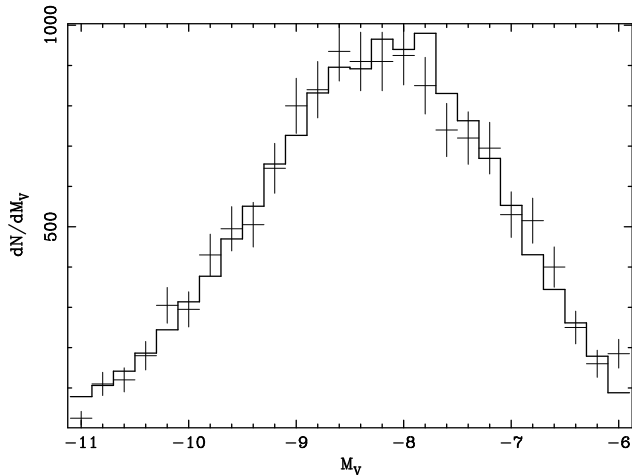


FIG. 6.— Composite GCLF for all the galaxies in the sample. Also shown is the best-fitting single Gaussian model, corrected for source detection incompleteness. Although the data are fitted with the Cash-C statistic, to guide the eye we show error-bars estimated from the Gehrels’ approximation. This demonstrates the good quality of a Gaussian GCLF fit to the data.

TABLE 4  
RADIAL DISTRIBUTION FITS

Galaxy	$\alpha_{Red}$	$\alpha_{Blue}$
NGC1332	$-1.5^{+0.2}_{-0.1}$	$-0.98^{+0.21}_{-0.18}$
NGC1399	$-0.73 \pm 0.23$	$-0.59 \pm 0.17$
NGC3115	$-0.54^{+0.44}_{-0.36}$	$-0.088^{+0.45}_{-0.38}$
NGC3585	$-0.71^{+0.73}_{-0.52}$	$-0.94^{+0.34}_{-0.28}$
NGC3607	$-1.1^{+0.6}_{-0.4}$	$-1.1 \pm 0.2$
NGC4125	$-0.26^{+0.41}_{-0.35}$	$-0.81 \pm 0.23$
NGC4261	$-0.90^{+0.30}_{-0.25}$	$-0.91^{+0.20}_{-0.18}$
NGC4365	$-0.79 \pm 0.29$	$-0.66^{+0.20}_{-0.18}$
NGC4472	$-0.61 \pm 0.24$	$-0.21 \pm 0.27$
NGC4494	$-0.97 \pm 0.18$	$-0.82^{+0.47}_{-0.38}$
NGC4552	$-1.1 \pm 0.2$	$-0.62 \pm 0.23$
NGC4621	$-0.58^{+0.40}_{-0.33}$	$-0.85 \pm 0.22$
NGC4649	$-0.42 \pm 0.28$	$-0.58 \pm 0.19$
NGC5846	$-1.0 \pm 0.2$	$-0.87^{+0.21}_{-0.18}$

NOTE. — Results from a power-law fit to the radial distribution of the GCs within a radius of  $1.5'$ . The power-law index,  $\alpha$  is given separately for the red and blue GCs. The distribution of blue GCs tends to be flatter than for red GCs.

would be detected in each bin.

We show the spatial distributions of a sub-sample of the galaxies, with sufficient measured GCs to yield interesting constraints, in Fig 7. We compare in this figure these distributions to the optical light, as parameterized by a de Vaucouleurs model, with its effective radius fixed to that measured in the K-band from the 2MASS Extended Source Catalog (Jarrett 2000). We found that both the red and blue GC distributions were significantly flatter than the optical light. These data could be fitted adequately by a single powerlaw model,

$$\frac{dn_{GC}}{dr} = N r^{1+\alpha} \quad (4)$$

where  $dn_{GC}/dr$  is the number density of GCs as a function of radius,  $r$ , and  $\alpha$  is a parameter of the fit, as is the

normalization  $N$ . The results of the fits are tabulated in Table 4 and shown in Fig 7. The GC distributions are considerably flatter than typically reported for studies with larger radial coverage (e.g. Kissler-Patig 1997, and references therein), but this simply reflects the flattening of the GC distributions in the galaxy core (e.g. Bassino et al. 2006). In general, the red GCs are significantly more centrally-peaked than the blue GCs, although there were a few exceptions to this trend. This is probably a result of the size of the error-bars, the lack of full azimuthal coverage, the relatively small numbers of sources detected and, critically, the small radial range. In any case, on average, the index for the blue GC radial distribution is less negative by  $\sim 0.15$ .

## 6. DISCUSSION

In order to facilitate a direct comparison between LMXBs in early-type galaxies and possible GC candidates, we have presented a catalogue of GC candidates and key derived properties based on the *HST* WFPC2 centrally-pointed observations of 19 nearby early-type galaxies. The complete source catalogue, including coordinates and photometry, is given in Appendix B. The total fraction of the GC light detected and GC specific luminosities are given for each galaxy in Table 2. In Paper I we combine these data with archival *Chandra* observations of early-type galaxies to show that the majority of LMXBs must have formed in GCs.

We self-consistently derived various properties of the GC populations, including fits to the GCLFs. We report specific frequency,  $S_N$ , and specific luminosity,  $S_L$ , of the GC populations. Since the luminosity is dominated by clusters brighter than the turnover, we found that  $S_L$  is much less sensitive than  $S_N$  to uncertainties in the GCLF turnover or width, making it a more robust indicator of the richness of the GC population where a significant fraction of the GCs are undetected due to source detection incompleteness. We find that the absolute magnitude of the GCLF turnover ( $M_V^T$ ) exhibits intrinsic scatter from galaxy to galaxy of  $\sim 0.3$ – $0.4$  mag, when compared to SBF distance moduli, consistent with the estimate of Ferrarese et al. (2000). Kundu & Whitmore (2001a) argued the intrinsic uncertainty in the GCLF distance measure is  $\sim 0.14$  mag, but only when using a small subset of the galaxies in their sample with the smallest error-bars on  $m_V^T$ . However, there is a significant correlation between  $(m_V^T - m_{V,model}^T)$  and the error on  $m_V^T$  (as expected, since, the fainter the turnover, the less complete the data), and so this systematically selects against galaxies with faint  $M_V^T$ , possibly reducing the scatter. Provided their error-estimates are reasonably representative, one can adopt the procedure outlined in § 3.2 to estimate the intrinsic scatter for the 25 galaxies in their full sample which overlap the SBF sample of Tonry et al. (2001). Using this approach, we estimate an intrinsic scatter of  $\sim 0.38$  mag (with a 90% lower limit of 0.23 mag), consistent with our results. Jordán et al. (2006) (see also Jordán et al. 2007) fitted Gaussian models to the GCLFs of early-type galaxies in Virgo, and found a trend of increasingly faint turnover magnitude with fainter  $M_B$ . For their galaxies with  $M_B \lesssim -20$ , we estimate by eye an intrinsic scatter of  $\sim 0.3$  mag, also consistent with the estimate from our data. To some ex-

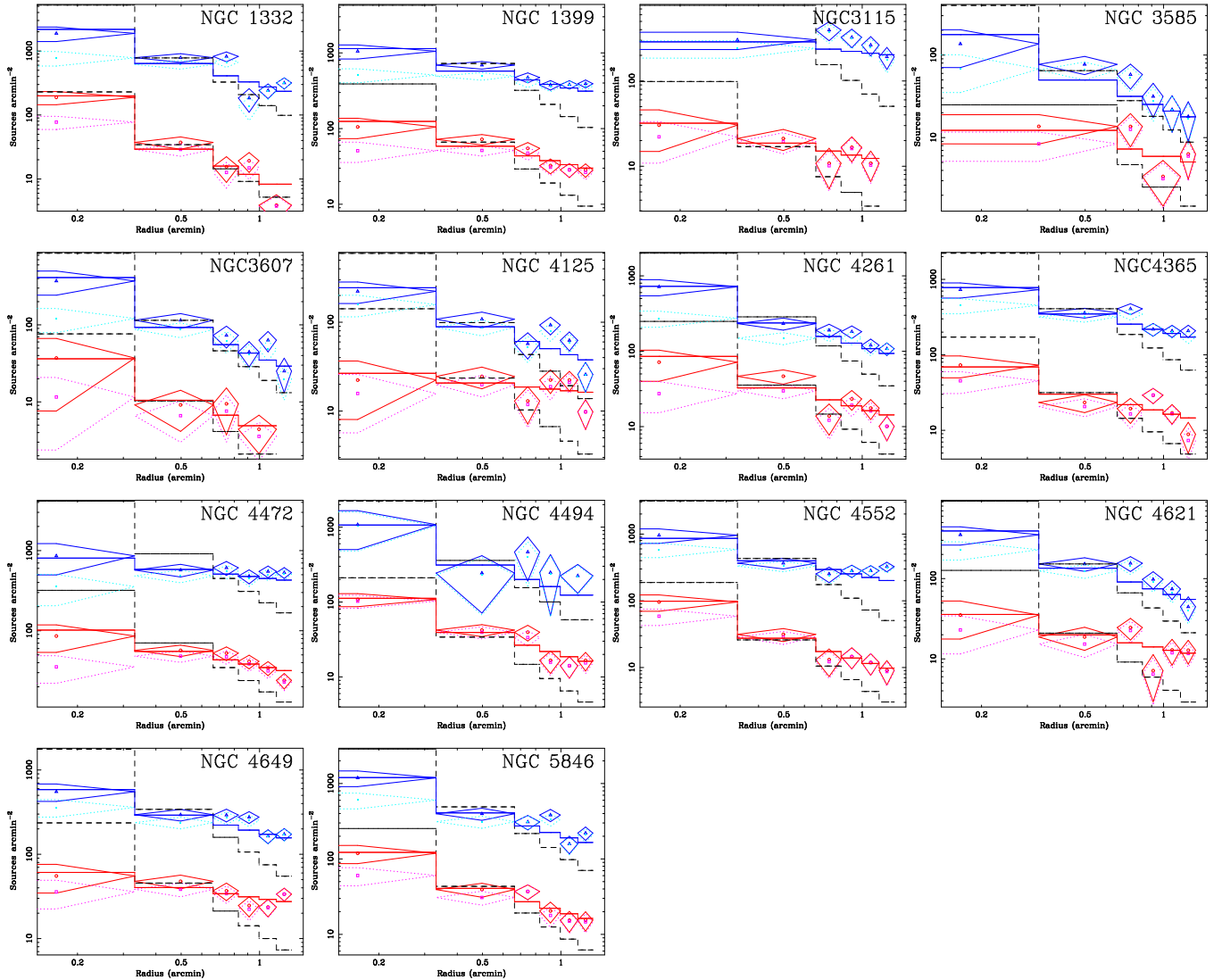


FIG. 7.— Azimuthally-averaged radial distribution of the GCs in a sub-sample of the galaxies. The radial distribution of the blue GCs are displaced upwards by an arbitrary amount for clarity. The measured radial profiles data-points (solid lines) have been corrected for source detection incompleteness. We also show these data without correction (dotted lines). In addition, we show (dashed line; black) the distribution of K-band optical light, and the best-fit simple powerlaw models to each dataset. In general, the GC distribution is flatter than the optical light, and the blue GCs tend to have a flatter distribution than the red GCs.

tent, this scatter is driven by the presence of significant populations of diffuse star clusters in two systems; it may be that the presence of similar populations in the galaxies we consider here have contributed to the significant scatter we observe.

In keeping with past studies of GCs using V and I-band photometry we did not find any evidence of a significant correlation between colour and luminosity. Converting the colour and magnitude of each GC to mass and metallicity, however, we found evidence of a weak mass-metallicity correlation for the GC populations as a whole. This trend cannot simply be attributed to observational biases, such as the systematic failure to detect faint (low-mass), red (metal-rich) GCs, since that would actually result in a stronger correlation in the colour-magnitude diagram. Similarly, our assumptions of a constant age for all GCs or a blue horizontal branch for all GCs do not appear to bias our results.

The apparent contradiction of no colour-magnitude correlation implying a mass-metallicity relation can be

understood in terms of the weak dependence of the SSP mass-to-light ratio on the metallicity. To put this another way, if there was no correlation between mass and metallicity, due to the dependence of the mass-to-light ratio on metallicity, we would expect there to be a significant colour-magnitude correlation. To investigate this further, we simulated an artificial dataset comprising a similar number of GCs to that observed. For each artificial GC, we randomly assigned a mass and metallicity value from, respectively, uncorrelated log-normal and normal distributions which approximately matched the observed data. Using the appropriate V and I-band mass-to-light ratios from Maraston (2005), these data were converted to V and I-band photometry, and estimated experimental noise was added. There was strong evidence of a weak correlation (the probability of no correlation was  $< 10^{-40}$ ) between colour and magnitude, with the fainter GCs being, on average redder. Conversely, we have also used similar simulations to generate colour-magnitude diagrams from artificial GC datasets

which obey the observed mass-metallicity dependence. Exactly as expected, we find that there is only weak evidence of a correlation in the resulting data (prob of no correlation  $\sim 0.1\%$ , as compared to  $\sim 10^{-37}$  in colour-metallicity space), demonstrating that the metallicity-dependent mass-to-light ratio can, indeed, destroy a colour-magnitude relation.

The galaxies in our sample span a range of magnitudes and so it is important to consider whether the known correlation between the galaxy mass and the peak of the GC colour distribution may affect our results. In part the relation reflects the increasing importance of red clusters in higher-mass galaxies (e.g. Peng et al. 2006) and it is difficult to imagine how that could introduce a spurious GC mass-metallicity correlation if one is not already present. More problematically though, Peng et al. report a correlation between the mean metallicity of the *blue* GCs and the galaxy mass and a similar trend for the red clusters. However, lower-mass galaxies are observed to have systematically narrower and fainter GCLFs (Jordán et al. 2007), which would be consistent with a trend for brighter GCs to be redder. In any case, for the magnitude range of the galaxies we consider here, the scatter about each correlation is at least as large as the trend.

After this work was submitted for publication, we became aware of a paper by Kundu (2008) which suggests that an apparent mass-metallicity relation may arise due to observational biases. He proposes that a weak mass-radius relationship, coupled with differing errors in the photometric aperture correction (since larger clusters may be marginally resolved) in different wavebands may lead to a spurious correlation. To investigate whether this could plausibly explain our observations, we first estimated the error in the aperture correction for both V and I band by convolving King models with varying half light radii ( $R_{1/2}$ ) with PSF images (as described in § 2). Since the vast majority of the GCs in our study were detected on the WF CCDs and in galaxies more distant than 15 Mpc, we computed the correction for our WF photometry only and adopted a 15 Mpc distance while allowing  $R_{1/2}$  to vary from 1 to 8 pc (consistent with observations, e.g. Spitler et al. 2006). Although the size of the cluster can affect the photometry in either band by as much as  $\sim 0.3$  mag, the effect was very similar in each filter so that V-I only changed by  $\ll 0.1$  mag. Such a small effect is not enough to wipe out the expected V-I *versus* V correlation in the case that mass and metallicity are uncorrelated. We have verified this by adding a colour-size relation into our Monte-Carlo simulations detailed above. We adopted a pathological monotonic linear relation between GC radius and V-band magnitude, which is much stronger than the weak trend observed. For our simulated colour-magnitude diagram under the assumption of no mass-metallicity relation, we found that, although the mass-radius effect slightly reduces the resulting colour-magnitude correlation, the probability the data are consistent with no correlation is still  $\sim 10^{-32}$ .

While our results depend to some degree on the adopted SSP models, it is clear that two independent sets of models—those of Maraston (2005) and those of Fioc & Rocca-Volmerange (1997) both imply a significant correlation between the mass and metallicity in these objects. The different normalizations and slopes for these models

simply arise from differences in the predicted relations between the V and I-band mass-to-light ratios and the metallicity between the sets of models. However, *any* prediction of a metallicity-dependent mass-to-light ratio will clearly give rise to a mass-metallicity correlation of this kind.

It is also interesting to compare our best-fitting mass-metallicity relation with that observed in early-type galaxies. We show in Fig 2 an extrapolation of the best-fitting straight-line relation for early-type galaxies found by Thomas et al. (2005). Intriguingly, we find a reasonable qualitative agreement, although the Thomas et al. relation is slightly less steep and has a slightly higher normalization. The observed trend for GCs may arise from a number of effects, such as self-enrichment (e.g. Mieske et al. 2006), in which the deeper potential wells of more massive GCs are more able to hold onto metals ejected from the very first generations of stars within them than in less-massive systems. Alternatively, the mass of a forming GC may be related to the mass (and metallicity) of its parent gas cloud (e.g. Harris et al. 2006). Whatever processes actually underlie the mass-metallicity relation, the remarkable amount of intrinsic scatter (0.6 dex in metallicity) implies that stochastic processes actually dominate in determining the metallicity of an individual GC. Alternatively if there are, in fact, metal-rich and metal-poor sub-populations that cannot be distinguished in our data due to the statistical noise, and which exhibit different relations, the measured scatter will actually substantially overestimate the magnitude of such effects.

Recent (B,I)-band photometry, which allows better separation of metal-rich and metal-poor clusters, has revealed colour-magnitude correlations for the metal-poor (blue) sub-population of GCs in some early-type galaxies, but no clear trend for the red population. Transforming a composite colour-magnitude diagram of three giant Virgo ellipticals onto the mass-metallicity plane, Mieske et al. (2006) found little evidence of bimodality, but a trend of increasing average metallicity with mass, broadly consistent with our observed mass-metallicity dependence. Although bimodal colour distributions need not necessarily imply bimodal metallicity distributions (e.g. Richtler 2006), it is unclear whether the absence of bimodality in the mass-metallicity plane is simply an artefact of noise introduced during the transformation from colour-magnitude space. In particular, for our data, the error-bars on  $[Z/H]$  were typically so large that two putative distinct populations may have been blurred together. This is particularly relevant when we consider whether the “blue tilt” and, in particular, the lack of a colour-magnitude relation for the metal-rich clusters found by previous authors, are consistent with our data. To assess this, we simulated a set of artificial GC photometry data-points in the (g,z) photometric bands, with random z-band absolute magnitudes ranging from -7 to -11 and colours obeying the “blue tilt” relation found for blue GCs by Strader et al. (2006). Transforming the data to the mass-metallicity plane using the models of Maraston (2005), the data were approximately consistent with a simple linear relation of the form  $[Z/H] = 4.43 + 0.50 \log_{10}(M/M_{\odot})$ . Performing the same analysis for the red GCs found by Strader et al., which we approximate as having g-z colours of 1.4, we found  $[Z/H] \simeq -0.22$ .

For a population of both blue and red GCs, we would expect the mean mass-metallicity relation to be simply a weighted average of these two relations. The existing best-fit slope and intercept are actually reproduced fairly well (0.25 and -2.3, respectively) for a (reasonable) blue

GC fraction of  $\sim 50\%$ . This excellent agreement with our results indicates that we may be observing the same trend as was observed in the (g,z) band, albeit the different trends for the red and blue populations are averaged together.

#### APPENDIX

##### FITTING THE GCLF WITH A RESPONSE MATRIX

Our method to fit the GCLF took account of both the source detection incompleteness and the effects of the Eddington bias by adapting the “response matrix” formalism from X-ray astronomy (e.g. Davis 2001). Wang (2004) used a similar, but not identical, method to correct for the Eddington bias when fitting luminosity functions of X-ray binaries. For each galaxy we have a set of measured GC magnitudes (and intrinsic errors on the measured magnitudes), which we binned into an arbitrary set of bins. The resulting histogram can be written as  $D_i$  ( $i = 1 \dots n$ ). Consider a GC with an intrinsic magnitude  $m$ , which we *measure* and assign to one of these bins. Due to statistical fluctuations there is a finite possibility that it will be detected in any one of the bins  $1 \dots n$  (or not at all). We can therefore define  $p_i(m)$  as the probability that this object is detected in bin  $i$ . If the differential GCLF can be written  $dn/dm$ , it follows that:

$$\langle D_i \rangle = \int_{-\infty}^{+\infty} dm p_i(m) \frac{dn}{dm}(m)$$

where the angle brackets denote the expectation. We can approximate this integral as a sum:

$$\langle D_i \rangle \simeq \sum_{j=1}^N p_{ij} \int_{m_{j-1}}^{m_j} dm \frac{dn}{dm}(m) \equiv \sum_{j=1}^N p_{ij} f_j$$

where  $p_{ij} = p_i(m_j)$ , and the spacing between each  $m_j$  ( $j = 1 \dots N$ ) is small enough to ensure that  $p_i(m)$  does not vary strongly between them. For any given parameterized GCLF, we therefore have the expected number of GCs in each bin  $i=1 \dots n$ , allowing us to construct a likelihood function after Cash (1979). Maximizing the likelihood function enables the parameters which define the GCLF shape to be constrained by the data.

The probability  $p_{ij}$  is, in principle, dependent on the measurement errors, source confusion and the “background” level (which varies strongly across the image) so its computation from first principles is extremely demanding. Instead, we choose to estimate it by adding objects of known intrinsic magnitude  $m_k$  to the image and measuring them from the data. Since this is equivalent to setting  $f_j = \delta_{jk}$ , where  $\delta_{jk}$  is the Kronecker delta function, it follows that  $\langle D_i \rangle = p_{ik}$ . For each magnitude  $m_k$ , we added 100 stars in this manner to the image (as described in § 4.1), and assumed that the arithmetic mean of our *measured*  $D_i$  recovered for those stars was a good approximation for the expectation in order to estimate  $p_{ik}$ . The accuracy of this assumption is dependent on the number of simulations performed and so we expect some intrinsic inaccuracy in our measured probabilities which, in turn, may affect the likelihood function and derived parameters. It is therefore important to assess whether 100 simulations are sufficient for our purposes.

To assess the accuracy of the matrices  $p_{ij}$ , we performed a set of Monte-Carlo simulations to determined how accurately a known GCLF can be recovered. We adopted an arbitrary analytical expression for the incompleteness as a function of measured magnitude, which was chosen approximately to match the behaviour found for a representative galaxy in our sample, NGC 4365. We stress that we do not have to match exactly the properties of the galaxy, only approximately for our present purposes. Adopting measurement errors consistent with the observed data, we were able to simulate an “observed” dataset, given a known input luminosity function. In this way, we were also able to generate corresponding response matrices, following the procedure described in § 4.1. We generated matrices using 100 simulated sources per magnitude bin, as in § 4.1 but also generated a separate set of matrices using 10000 sources per magnitude bin. We subsequently refer to these as the standard and large matrices, respectively.

We carried out 100 Monte Carlo simulations, on each of which we generated both a dataset and corresponding response matrices, binned identically to the real data. For the input GCLF, we assumed  $m_V^T = 24.0$ ,  $\sigma_V = 1.3$ , consistent with NGC 4365, and a total number of 500 GCs. For each dataset and response matrix pair, we fitted the simulated data, allowing both  $m_V^T$  and the normalization to fit freely. The mean and standard error of the best-fitting parameters, averaged over the simulations, can be used to assess the bias and statistical error (which will also include a contribution from the error on the response matrix due to the finite number of simulated sources used to create it) implicit in our analysis. Applying the standard matrices, we obtained best-fitting  $m_V^T = 24.00 \pm 0.12$  ( $1-\sigma$  error) and a normalization of  $504 \pm 41$  ( $1-\sigma$ ) GCs. The best-fitting values are sufficiently close to the true value to indicate that the results are not biased, and the recovered errors are broadly consistent with those found for the real data. Adopting the large matrices, we recovered best-fitting values of  $m_V^T = 24.02 \pm 0.11$  ( $1-\sigma$  errors) and a normalization of  $506 \pm 36$  ( $1-\sigma$ ) GCs. Since increasing the number of simulations used to generate the matrices by a factor 100 has virtually no impact on the recovered parameters or error bars, it follows that the standard matrices are sufficient to fit the GCLF.

As another way to assess the accuracy of the matrices, we also performed a set of simulations for each dataset, in which the response matrix was replaced with an artificial matrix,  $p'_{ij}$ , which was derived from the real matrix, with approximately the expected level of statistical noise added (assuming the “observed”  $p_{ij}$  is exactly correct), and the data refitted. We performed 25 such simulations for each object and adopted the  $1-\sigma$  scatter of the best-fitting

TABLE 5  
CATALOGUE OF GC CANDIDATES

Source	RA	dec	V mag	I mag	Mass $10^6 M_{\odot}$	[Z/H]
<b>NGC 1332</b>						
1	03h26m17.34s	-21°20'25.5''	21.93 ± 0.04	20.79 ± 0.03	2.6 <sup>+0.5</sup> <sub>-0.3</sub>	-0.23 <sup>+0.15</sup> <sub>-0.28</sub>
2	03h26m16.94s	-21°20'16.7''	23.9 ± 0.2	22.9 ± 0.2	0.28 <sup>+0.27</sup> <sub>-0.05</sub>	-1.2 <sup>+0.6</sup> <sub>-1.0</sub>
3	03h26m17.38s	-21°20'18.4''	23.4 ± 0.1	21.99 ± 0.09	1.11 ± 0.07	0.67 <sup>+0.010</sup> <sub>-0.23</sub>
4	03h26m17.58s	-21°20'18.9''	22.64 ± 0.08	21.36 ± 0.06	2.08 <sup>+0.09</sup> <sub>-0.2</sub>	0.44 <sup>+0.23</sup> <sub>-0.16</sub>
5	03h26m17.82s	-21°20'19.1''	23.4 ± 0.1	22.22 ± 0.09	0.69 ± 0.15	-0.22 <sup>+0.77</sup> <sub>-0.30</sub>

NOTE. — The complete version of this table is in the electronic edition of the Journal. The printed edition contains only a sample.

parameters from our Monte-Carlo simulations as an estimate of the uncertainty arising from our matrix calculation. We computed  $p'_{ij}$  in the following manner. For each magnitude  $m_j$ , we drew 100 sources which were distributed amongst the histogram data-bins  $i=1..n$  randomly but following the probability distribution  $p_{ij}$ . Denoting the resulting data histogram as  $(D'_i)_j$ , clearly  $\langle (D'_i)_j \rangle = 100p_{ij}$  (since there are 100 sources). The actual values of  $(D'_i)_j$  will be distributed about this expectation due to statistical scatter, allowing us to define  $p'_{ij} = (D'_i)_j/100$ . In practice, we found the uncertainty arising from the matrix computation for  $S_N$ ,  $S_L$  and  $m_V^T$  to be  $\lesssim 10\%$ ,  $\lesssim 4\%$  and  $\lesssim 1\%$ , respectively, which are far smaller than any other source of error in our calculations for these quantities.

#### SOURCE LISTS AND PHOTOMETRY

We show in Table 5 a list of the GC candidates detected in each galaxy. For each source, we provide a unique identification number within that galaxy, as well as its right ascension and declination. We provide the V and I-band photometry for each candidate GC as well as the mass and metallicity, having converted them using the SSP models of Maraston (2005), assuming an age of 13 Gyr and a blue horizontal branch. All errors are quoted at the 1- $\sigma$  confidence level. Note that [Z/H] is constrained to lie in the range covered by the models, i.e. -2.25 to 0.67.

We would like to thank David Buote, Fabio Gastaldello and Luca Zappacosta for stimulating discussions. We would like to thank Marc Seigar and Aaron Barth for helpful discussions regarding the analysis of the *HST* data. Some of the data presented in this paper were obtained from the Multimission Archive at the Space Telescope Science Institute (MAST). STScI is operated by the Association of Universities for Research in Astronomy, Inc., under NASA contract NAS5-26555. This research has also made use of the NASA/IPAC Extragalactic Database (*NED*) which is operated by the Jet Propulsion Laboratory, California Institute of Technology, under contract with NASA, and the HyperLEDA database (<http://leda.univ-lyon1.fr>). Support for this work was provided by NASA under grant NNG04GE76G issued through the Office of Space Sciences Long-Term Space Astrophysics Program.

#### REFERENCES

- Bassino, L. P., Richtler, T., & Dirsch, B. 2006, *MNRAS*, 367, 156  
 Brodie, J. P. & Huchra, J. P. 1991, *ApJ*, 379, 157  
 Brodie, J. P. & Strader, J. 2006, *ARA&A*, 44, 193  
 Cardelli, J. A., Clayton, G. C., & Mathis, J. S. 1989, *ApJ*, 345, 245  
 Carpenter, J. M. 2001, *AJ*, 121, 2851  
 Cash, W. 1979, *ApJ*, 228, 939  
 Clark, G. W. 1975, *ApJ*, 199, L143  
 Davis, J. E. 2001, *ApJ*, 548, 1010  
 de Vaucouleurs, G., de Vaucouleurs, A., Corwin, H. G., Buta, R. J., Paturel, G., & Fouque, P. 1991, *Third Reference Catalogue of Bright Galaxies* (Volume 1-3, XII, 2069 pp. 7 figs.. Springer-Verlag Berlin Heidelberg New York)  
 Faber, S. M., Wegner, G., Burstein, D., Davies, R. L., Dressler, A., Lynden-Bell, D., & Terlevich, R. J. 1989, *ApJS*, 69, 763  
 Fabian, A. C., Pringle, J. E., & Rees, M. J. 1975, *MNRAS*, 172, 15P  
 Ferrarese, L., et al. 2000, *ApJ*, 529, 745  
 Fioc, M. & Rocca-Volmerange, B. 1997, *A&A*, 326, 950  
 Fioc, M. & Rocca-Volmerange, B. 1999, *astro-ph/9912179*  
 Gebhardt, K. & Kissler-Patig, M. 1999, *AJ*, 118, 1526  
 Geisler, D., Lee, M. G., & Kim, E. 1996, *AJ*, 111, 1529  
 Grindlay, J. E. 1987, in *IAU Symposium*, Vol. 125, *The Origin and Evolution of Neutron Stars*, ed. D. J. Helfand & J.-H. Huang, 173–184  
 Harris, W. E. 1991, *ARA&A*, 29, 543  
 Harris, W. E., Whitmore, B. C., Karakla, D., Okoń, W., Baum, W. A., Hanes, D. A., & Kavelaars, J. J. 2006, *ApJ*, 636, 90  
 Holtzman, J. A., Burrows, C. J., Casertano, S., Hester, J. J., Trauger, J. T., Watson, A. M., & Worthey, G. 1995a, *PASP*, 107, 1065  
 Holtzman, J. A., et al. 1995b, *PASP*, 107, 156  
 Humphrey, P. J. & Buote, D. A. 2004, *ApJ*, 612, 848  
 Humphrey, P. J. & Buote, D. A. 2006, *ApJ*, 639, 136  
 Humphrey, P. J. & Buote, D. A. 2008, *ApJ*, in press, [astro-ph/0612058](http://astro-ph/0612058)  
 Humphrey, P. J., Buote, D. A., Gastaldello, F., Zappacosta, L., Bullock, J. S., Brighenti, F., & Mathews, W. G. 2006, *ApJ*, 646, 899  
 Irwin, J. A. 2005, *ApJ*, 631, 511  
 Ivanova, N. 2006, *ApJ*, 636, 979  
 Jacoby, G. H., Branch, D., Clardullo, R., Davies, R. L., Harris, W. E., Pierce, M. J., Pritchet, C. J., Tonry, J. L., & Welch, D. L. 1992, *PASP*, 104, 599  
 Jarrett, T. H. 2000, *PASP*, 112, 1008  
 Jensen, J. B., Tonry, J. L., Barris, B. J., Thompson, R. I., Liu, M. C., Rieke, M. J., Ajhar, E. A., & Blakeslee, J. P. 2003, *ApJ*, 583, 712  
 Jordán, A., Côté, P., Ferrarese, L., Blakeslee, J. P., Mei, S., Merritt, D., Milosavljević, M., Peng, E. W., Tonry, J. L., & West, M. J. 2004, *ApJ*, 613, 279

- Jordán, A., McLaughlin, D. E., Côté, P., Ferrarese, L., Peng, E. W., Mei, S., Villegas, D., Merritt, D., Tonry, J. L., & West, M. J. 2007, *ApJS*, 171, 101
- Jordán, A., et al. 2006, *ApJ*, 651, L25
- Juett, A. M. 2005, *ApJ*, 621, L25
- Kim, E., Kim, D.-W., Fabbiano, G., Lee, M. G., Park, H. S., Geisler, D., & Dirsch, B. 2006, *ApJ*, 647, 276
- King, I. 1962, *AJ*, 67, 471
- Kissler-Patig, M. 1997, *A&A*, 319, 83
- Kroupa, P. 2001, *MNRAS*, 322, 231
- Kundu, A. 2008, *AJ*, 136, 1013
- Kundu, A., Maccarone, T. J., & Zepf, S. E. 2002, *ApJ*, 574, L5
- Kundu, A. & Whitmore, B. C. 2001a, *AJ*, 121, 2950
- Kundu, A. & Whitmore, B. C. 2001b, *AJ*, 122, 1251
- Kundu, A., Whitmore, B. C., Sparks, W. B., Macchetto, F. D., Zepf, S. E., & Ashman, K. M. 1999, *ApJ*, 513, 733
- Larsen, S. S., Brodie, J. P., Huchra, J. P., Forbes, D. A., & Grillmair, C. J. 2001, *AJ*, 121, 2974
- Maccarone, T. J., Kundu, A., & Zepf, S. E. 2004, *ApJ*, 606, 430
- Maraston, C. 1998, *MNRAS*, 300, 872
- Maraston, C. 2005, *MNRAS*, 362, 799
- Mieske, S., et al. 2006, *ApJ*, 653, 193
- Peng, E. W., Jordán, A., Côté, P., Blakeslee, J. P., Ferrarese, L., Mei, S., West, M. J., Merritt, D., Milosavljević, M., & Tonry, J. L. 2006, *ApJ*, 639, 95
- Press, W. H., Teukolsky, S. A., Vetterling, W. T., & Flannery, B. P. 1992, *Numerical Recipes in C: The Art of Scientific Computing*. Second Ed. (C.U.P.)
- Richtler, T. 2006, *Bulletin of the Astronomical Society of India*, 34, 83
- Sarazin, C. L., Kundu, A., Irwin, J. A., Sivakoff, G. R., Blanton, E. L., & Randall, S. W. 2003, *ApJ*, 595, 743
- Schlegel, D. J., Finkbeiner, D. P., & Davis, M. 1998, *ApJ*, 500, 525
- Sivakoff, G. R., Jordán, A., Sarazin, C. L., Blakeslee, J. P., Côté, P., Ferrarese, L., Juett, A. M., Mei, S., & Peng, E. W. 2007, *ApJ*, 660, 1246
- Smits, M., Maccarone, T. J., Kundu, A., & Zepf, S. E. 2006, *A&A*, 458, 477
- Spitler, L. R., Larsen, S. S., Strader, J., Brodie, J. P., Forbes, D. A., & Beasley, M. A. 2006, *AJ*, 132, 1593
- Strader, J., Brodie, J. P., Spitler, L., & Beasley, M. A. 2006, *AJ*, 132, 2333
- Thomas, D., Maraston, C., & Bender, R. 2003, *MNRAS*, 339, 897
- Thomas, D., Maraston, C., Bender, R., & de Oliveira, C. M. 2005, *ApJ*, 621, 673
- Tonry, J. L., Dressler, A., Blakeslee, J. P., Ajhar, E. A., Fletcher, A., Luppino, G. A., Metzger, M. R., & Moore, C. B. 2001, *ApJ*, 546, 681
- Tremaine, S., et al. 2002, *ApJ*, 574, 740
- van Dokkum, P. G. 2001, *PASP*, 113, 1420
- Vesperini, E. & Zepf, S. E. 2003, *ApJ*, 587, L97
- Wang, Q. D. 2004, *ApJ*, 612, 159
- Yoon, S.-J., Yi, S. K., & Lee, Y.-W. 2006, *Science*, 311, 1129
- Zepf, S. E. & Ashman, K. M. 1993, *MNRAS*, 264, 611